

Productions of J/ψ mesons in p -Pb collisions at 5 TeV

Fu-Hu Liu^{a,1}, Hai-Ling Lao^a, and Roy A. Lacey^{b,2}

^a*Institute of Theoretical Physics, Shanxi University, Taiyuan, Shanxi 030006, China*

^b*Departments of Chemistry & Physics, Stony Brook University, Stony Brook, NY 11794, USA*

Abstract: The rapidity distributions of J/ψ mesons produced in proton-lead (p -Pb) collisions at center-of-mass energy per nucleon pair $\sqrt{s_{NN}} = 5$ TeV are studied by using a multisource thermal model and compared with the experimental data of the LHCb and ALICE Collaborations. Correspondingly, the pseudorapidity distributions are accurately obtained from the parameters extracted from the rapidity distributions. At the same time, the transverse momentum distributions in the same experiments are described by the simplest Erlang distribution which is the folding result of two exponential distributions which are contributed by the target and projectile partons respectively.

Keywords: Rapidity distribution, transverse momentum distribution, p -Pb collisions

PACS Nos: 25.75.-q, 24.10.Pa, 25.75.Dw

1 Introduction

The successful running of the Large Hadron Collider (LHC) at the European Organization for Nuclear Research (CERN) has been advancing heavy ion (nucleus-nucleus) collisions from GeV to TeV energies [1–4]. It is already established that a new state of matter, namely the Quark-Gluon Plasma (QGP), has been formed in nucleus-nucleus collisions at high energies due to high temperature and density [5–11]. As one of the most valuable signatures of the formation of QGP, the suppression of J/ψ mesons produced in nucleus-nucleus collisions has been studied [12–15]. In fact, the suppression of J/ψ mesons can also be found in proton-nucleus (pA) collisions, where the QGP is not expected to produce [16] due to small system. Instead, some cold nuclear matter effects such as nuclear absorption and shadowing as well as parton energy loss affect the productions of final-state particles in pA collisions [17–19]. In addition, at LHC energies, it is well established by now that the situation is much more involved, with recombination processes playing an essential role [20, 21].

Except for the production of QGP in high energy nucleus-nucleus collisions, other topics such as some universal laws and particular properties of measurable quantities in intermediate and high energy particle-particle, particle-nucleus, and nucleus-nucleus collisions are interested for the community of particle and nuclear physics. These universal

¹E-mail: fuhuli@163.com; fuhuli@sxu.edu.cn

²E-mail: Roy.Lacey@Stonybrook.edu

laws and particular properties are expected to exist in transverse momentum distribution, multiplicity and transverse energy distribution, rapidity distribution and correlation, azimuthal distribution and correlation, fragment production, and so forth [22–26]. We have always been interested in the study of universal laws in different systems [22–24].

Recently, the productions of J/ψ mesons in proton-lead (p -Pb) collisions at LHC energies are studied. Some experimental results are obtained [16, 27–30]. We are interested in the rapidity (y) and transverse momentum (p_T) distributions of J/ψ mesons. From y distribution, we can test some models in the longitudinal rapidity space, and obtain some information on energy loss of partons and penetrating (stopping) power of projectile and target nuclei. From p_T distribution, we can test some models in the transverse momentum space and obtain excitation degree of the interacting system.

In this paper, by using a multisource thermal model [31–33], we study y and p_T distributions of J/ψ mesons produced in p -Pb collisions at center-of-mass energy per nucleon pair $\sqrt{s_{NN}} = 5$ TeV which is one of the LHC energies corresponding to a proton beam energy of 4 TeV and a lead beam energy of 1.58 TeV per nucleon. At the same time, the pseudorapidity (η) distributions of J/ψ mesons are obtained. In section 2, a description of the model and calculation method is presented. In section 3, the results and discussion are given. The calculated results are found to be in agreement with the available experimental data of the LHCb and ALICE Collaborations [16, 29, 30]. Finally, we summarize our main observations and conclusions in section 4.

2 The model and calculation method

The model employed in the present work is the multisource thermal model [31–33] which is a successor of the thermalized cylinder model [34, 35] which is based on the one-dimensional string model [36] and the fireball model [37]. According to the one-dimensional string model [36], in high energy nucleon-nucleon collisions, a string is formed consisting of two endpoints acting as energy reservoirs and the interior with constant energy per length. Because of the asymmetry of the mechanism, the string will break into many substrings along the direction of incident beam. According to the fireball model [37], in the mentioned collisions, the incident nucleon penetrates through the target nucleon, then a fire streak (a series of fireballs) is formed along the direction of incident beam. The distribution length of substrings in the one-dimensional string model [36] and the length of fire streak in the fireball model [37] will define the width of the (pseudo)rapidity distribution. In high energy nucleus-nucleus collisions, many strings or fire streaks are formed along the incident direction. Finally, a thermalized cylinder is formed because of these strings or fire streaks mix in the transverse direction.

Due to different excitation degrees of substrings or fireballs, the interacting system which contains many substrings or fireballs can be divided into several regions or sources. In addition, different interacting mechanisms or event samples can be resulted in different sources. Each source contains several sub-sources which can be substrings, fireballs, partons, or nucleons due to different topics of investigations such as the distributions of transverse momenta, multiplicities, rapidities, transverse energies, etc. Different sources can be described by the same law with different parameters or by different laws. The

distribution in final state is usually contributed by the several sources, which results in a multi-component distribution which results from the multisource thermal model.

In the framework of the considered model, most of light flavor particles such as pions and kaons can be regarded as a result of soft excitation process due to thermal reason. As heavy quark particle, J/ψ is produced inherently in a hard process which proceeds through parton-parton collisions. We assume that a parton in target nucleus (nucleon) and a parton in projectile nucleus (nucleon) take part in the collisions to form the source to emit J/ψ meson. Many sources can be formed in nucleus-nucleus collisions and in the considered data sample. These sources can appear in different regions in the interacting overlapping area. In rapidity space, in the laboratory or center-of-mass reference frame, these sources distribute at different rapidities (y_x) due to different rapidity shifts.

The sources with $y_x < 0$ are in the backward region which are mainly contributed by the target nucleus, and the sources with $y_x > 0$ are in the forward region which are mainly contributed by the projectile nucleus. The backward and forward regions are expected in $[y_T, 0]$ and $[0, y_P]$ respectively, where y_T (which is less than 0) and y_P (which is larger than 0) denote the maximum rapidity shifts in the backward and forward regions respectively, i.e. y_T is the minimum y_x and y_P is the maximum y_x . We would like to point out that the separation for the backward and forward regions does not mean that there is no source in the mid-rapidity region. In fact, these sources can also be divided into three groups: a central region with sources around the mid-rapidity, a target fragmentation region with sources in the target side, and a projectile fragmentation region with sources in the projectile side. The sources in the same region form a large source. Then, we have a three-source picture which is compatible with previous works [38–49].

Each parton (the i -th parton) is assumed to contribute an exponential transverse momentum (p_{Ti}) distribution with a mean value of $\langle p_{Ti} \rangle$. The mentioned distribution is

$$f_i(p_{Ti}) = \frac{1}{\langle p_{Ti} \rangle} \exp\left(-\frac{p_{Ti}}{\langle p_{Ti} \rangle}\right), \quad (1)$$

where $i = 1$ and 2 for the target parton and projectile parton respectively. Generally, $\langle p_{T1} \rangle = \langle p_{T2} \rangle = \langle p_{Ti} \rangle$. The p_T ($= p_{T1} + p_{T2}$) distribution of J/ψ is the folding result of two exponential distributions. We have p_T distribution to be the simplest Erlang distribution

$$f(p_T) = \int_0^{p_T} f_1(p_{T1}) f_2(p_T - p_{T1}) dp_{T1} = \int_0^{p_T} \frac{1}{\langle p_{Ti} \rangle^2} \exp\left(-\frac{p_T}{\langle p_{Ti} \rangle}\right) dp_{T1} = \frac{p_T}{\langle p_{Ti} \rangle^2} \exp\left(-\frac{p_T}{\langle p_{Ti} \rangle}\right). \quad (2)$$

In the Monte Carlo method, according to $\int_0^{p_{T1,2}} f_{1,2}(p_{T1,2}) dp_{T1,2} = R_{1,2}$, we have $p_{T1,2} = -\langle p_{Ti} \rangle \ln(1 - R_{1,2})$, where $R_{1,2}$ denote random numbers in $[0,1]$. Because of both $1 - R_{1,2}$ and $R_{1,2}$ being random numbers in $[0,1]$, we have

$$p_T = -\langle p_{Ti} \rangle (\ln R_1 + \ln R_2). \quad (3)$$

As a statistical result, in the source rest frame, we assume that J/ψ mesons are isotropically emitted, which results in the distribution of polar angle θ' being $\frac{1}{2} \sin \theta'$. Then, the polar angle θ' satisfies $\int_0^{\theta'} \frac{1}{2} \sin \theta' d\theta' = R_3$ in the Monte Carlo method, where R_3 denotes random numbers in $[0,1]$. We have θ' to be

$$\theta' = \arctan\left[\frac{2\sqrt{R_3(1-R_3)}}{1-2R_3}\right] + \theta_0, \quad (4)$$

where $\theta_0 = 0$ (or π) is for the case of the first term being larger than 0 (or less than 0) in Eq. (4). The longitudinal momentum p'_z and energy E' in the rest frame can be expressed as

$$p'_z = p_T \cot \theta' \quad (5)$$

and

$$E' = \sqrt{p_T^2 + p_z'^2 + m_0^2} \quad (6)$$

respectively, where m_0 denotes the rest mass of the considered particle.

In the laboratory or center-of-mass reference frame, the rapidity y , longitudinal momentum p_z , polar angle θ , and pseudorapidity η of the considered particle can be given by

$$y = \frac{1}{2} \ln \left(\frac{E' + p'_z}{E' - p'_z} \right) + y_x, \quad (7)$$

$$p_z = \sqrt{p_T^2 + m_0^2} \sinh y, \quad (8)$$

$$\theta = \arctan(p_T/p_z), \quad (9)$$

and

$$\eta = -\ln \tan(\theta/2), \quad (10)$$

respectively. The rapidity, pseudorapidity, and transverse momentum distributions are then given by the statistical method. In particular, for rapidity (pseudorapidity) distribution, the contribution fraction (relative contribution) k_T of the backward region and the contribution fraction $1 - k_T$ of the forward region may be different due to asymmetric p -Pb collisions.

3 Results and discussion

Fig. 1(a) presents the rapidity distributions, $d\sigma/dy$, of J/ψ mesons produced directly from the proton-nucleon collisions (prompt J/ψ) and from b -hadron decays (J/ψ from b) in p -Pb collisions at 5 TeV, where $d\sigma$ denotes the production cross-section of the considered J/ψ in rapidity bin dy . The symbols represent the experimental data of the LHCb Collaboration [16] and the curves are our fitting results based on the Monte Carlo calculation. In the calculations, for both the process of J/ψ productions, we take $\langle p_{Ti} \rangle = 1.50 \pm 0.10$ GeV/ c ; for the process of prompt J/ψ , we take $y_T = -4.41 \pm 0.40$, $y_P = 3.78 \pm 0.40$, $k_T = 0.58 \pm 0.06$, and $\sigma_0 = (5099.8 \pm 350.0)$ μb with χ^2 per degree of freedom (χ^2/dof) to be 1.394, where σ_0 denotes the total production cross-section of the considered J/ψ in full rapidity space; and for the process of J/ψ from b , we take $y_T = -3.86 \pm 0.40$, $y_P = 3.67 \pm 0.35$, $k_T = 0.50 \pm 0.04$, and $\sigma_0 = (629.2 \pm 41.0)$ μb with χ^2/dof to be 2.299. The normalization factor is in fact the production cross-section in full rapidity range. One can see that the model describes the experimental data of the LHCb Collaboration.

To see the characteristics of pseudorapidity distributions, the results corresponding to the curves in Fig. 1(a) are given in Fig. 1(b). Both the results for y and η distributions are direct and accurate. There is no conversion between them, where an unsuitable conversion may cause errors [52]. One can see large hollow structure in the region of $\eta = 0$. The

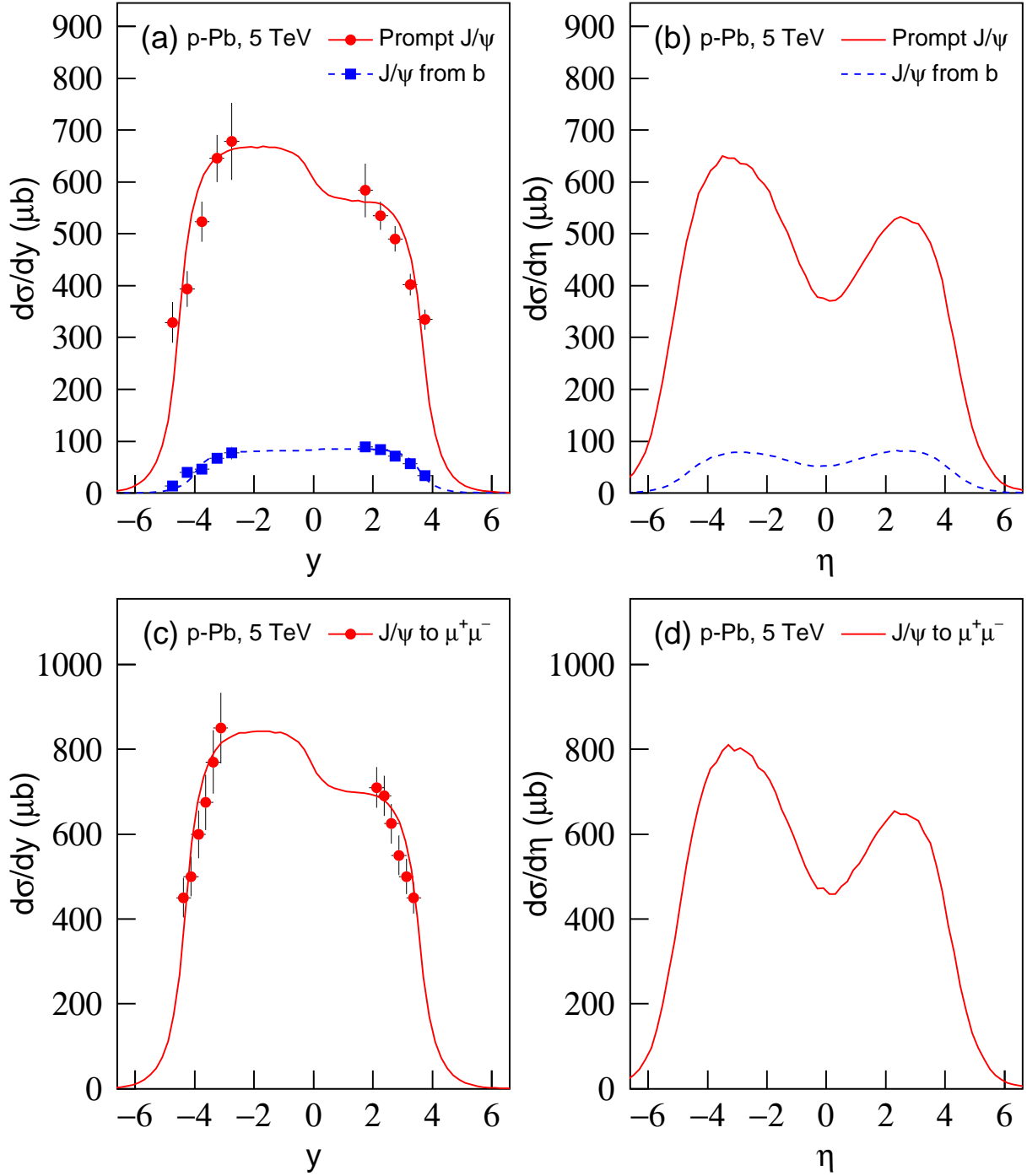


Fig. 1. (a) Rapidity distributions of prompt J/ψ and J/ψ from b in p -Pb collisions at 5 TeV. The symbols represent the experimental data of the LHCb Collaboration [16] and the curves are our calculated results. (b) Pseudorapidity distributions corresponding to the rapidity curves in Fig. 1(a). (c) Rapidity distributions of inclusive J/ψ to $\mu^+\mu^-$ in p -Pb collisions at 5 TeV. The symbols represent the experimental data of the ALICE Collaboration [29] and the curve is our calculated result. (d) Pseudorapidity distribution corresponding to the rapidity curve in Fig. 1(c).

difference between y and η is obvious for the production of heavy particles such as J/ψ . We cannot use $y \approx \eta$ in our calculation for heavy particles even at LHC energies.

Figs. 1(c) and 1(d) are similar to Figs. 1(a) and 1(b) respectively, but the former two are for inclusive J/ψ to $\mu^+\mu^-$ only. The symbols represent the experimental data of the ALICE Collaboration [29] and the curves are our modelling results. In the calculation, we take $\langle p_{Ti} \rangle = 1.40 \pm 0.08$ GeV/ c , $y_T = -4.20 \pm 0.40$, $y_P = 3.67 \pm 0.40$, $k_T = 0.58 \pm 0.06$, and $\sigma_0 = (6135.5 \pm 510.0)$ μb with χ^2/dof to be 0.454. One can see that the model describes the experimental data of the ALICE Collaboration. Again, the difference between y and η is obvious for the production of J/ψ .

From Figs. 1(a) and 1(c), one can see that the sources for the creations of prompt J/ψ , J/ψ from b , and inclusive J/ψ to $\mu^+\mu^-$ have nearly the same rapidity shift in the uncertainty range. For each creation, the rapidity shift in the backward region seems to be greater than that in the forward one, though large uncertainty range is used. Our calculation based on a revised nuclear-collision geometry [50] shows that the mean number of p -nucleon collisions in p -Pb collisions is 2.7. If the mean energy loss ratios in the first (or last) and other p -nucleon collisions are 98.28% and 52.20% respectively, which are about two times of those (50% and 25%) in fixed target experiments [51], the energies of each participant nucleon after collisions in the backward and forward regions are 1.58×0.0172 TeV and $4 \times 0.0172 \times 0.4780^{1.7}$ TeV, and the corresponding velocities β are $0.99940c$ and $0.99886c$, respectively. Thus, the mean rapidity shifts ($y = 0.5 \ln[(1 + \beta)/(1 - \beta)]$) in the backward and forward regions are -4.06 and 3.73 respectively, which are consistent to y_T and y_P respectively used in the present work.

Figs. 2(a) and 2(b) show the transverse momentum distributions, $d\sigma/dp_T$, of prompt J/ψ (and J/ψ from b) in rapidity ranges $1.5 < y < 4.0$ and $-5.0 < y < -2.5$ in p -Pb collisions at 5 TeV respectively. The symbols represent the experimental data of the LHCb Collaboration [16], the solid curves are our fitting results based on Eq. (2), and the dashed curves will be discussed later. The values of related parameters and χ^2/dof for the solid curves are presented in Table 1. One can see that the p_T distributions obey the simplest Erlang distribution. The value of $\langle p_{Ti} \rangle$ for prompt J/ψ is less than that for J/ψ from b , where the later one needs larger threshold energy for creation of b -hadron.

Figs. 2(c) and 2(d) are similar to Fig. 2(a), but the former two are for inclusive J/ψ to $\mu^+\mu^-$ and e^+e^- respectively, measured by the ALICE Collaboration [30] in different rapidity ranges shown in the panel and with alternative expression ($d^2\sigma/dydp_T$) of transverse momentum distribution. Particularly, in Fig. 2(d), only the solid curve based on Eq. (2) for J/ψ to e^+e^- is presented. The values of related parameters and χ^2/dof are listed in Table 1. Once again, the p_T distributions obey the simplest Erlang distribution. The value of $\langle p_{Ti} \rangle$ in large $|y|$ region is less than that in small $|y|$ region, where large angle scattering appears in small $|y|$ region which results in large p_T .

To see clearly the dependence of the transverse momentum distribution on rapidity, Figs. 3(a) and 3(b) present $d\sigma/dp_T$ versus p_T for prompt J/ψ and for J/ψ from b respectively, in different rapidity ranges. The symbols represent the experimental data of the LHCb Collaboration [16], the solid curves are our fitting results based on Eq. (2), and the dashed curves will be discussed later. For the purpose of clearness, the results for different rapidity ranges are multiplied by different amounts as marked in the panels. The values of related parameters and χ^2/dof for the solid curves are listed in Table 1. Once

more, the p_T distributions obey the simplest Erlang distribution. The value of $\langle p_{Ti} \rangle$ for prompt J/ψ is less than that for J/ψ from b , and both the values of $\langle p_{Ti} \rangle$ decrease with increase of the rapidity.

Table 1. Values of parameters and χ^2/dof corresponding to the solid curves in Figs. 2 and 3.

Fig.	Type or y range	$\langle p_{Ti} \rangle$ (GeV/c)	σ_0 (μb)	χ^2/dof
2(a)	prompt J/ψ	1.38 ± 0.08	1163.8 ± 120.4	0.632
	J/ψ from b	1.61 ± 0.13	165.2 ± 17.8	0.317
2(b)	prompt J/ψ	1.24 ± 0.05	1300.6 ± 138.1	0.954
	J/ψ from b	1.51 ± 0.11	114.0 ± 12.6	0.297
2(c)	$2.03 < y < 3.53$	1.42 ± 0.10	583.9 ± 60.3	0.505
	$-4.46 < y < -2.96$	1.25 ± 0.05	638.4 ± 58.5	0.529
2(d)	J/ψ to e^+e^-	1.45 ± 0.11	933.5 ± 90.2	0.013
3(a)	$1.5 < y < 2.0$	1.48 ± 0.10	585.4 ± 60.0	0.203
	$2.0 < y < 2.5$	1.49 ± 0.10	539.3 ± 52.9	0.308
	$2.5 < y < 3.0$	1.45 ± 0.09	488.0 ± 45.1	0.341
	$3.0 < y < 3.5$	1.33 ± 0.07	404.1 ± 40.3	0.559
	$3.5 < y < 4.0$	1.26 ± 0.06	337.8 ± 23.5	0.518
3(b)	$1.5 < y < 2.0$	1.74 ± 0.15	89.2 ± 9.9	0.120
	$2.0 < y < 2.5$	1.69 ± 0.14	84.1 ± 8.9	0.395
	$2.5 < y < 3.0$	1.61 ± 0.13	70.9 ± 6.7	0.402
	$3.0 < y < 3.5$	1.49 ± 0.10	55.8 ± 4.6	0.520
	$3.5 < y < 4.0$	1.47 ± 0.10	35.3 ± 3.4	0.357

In the above comparisons, each parton in J/ψ production contributes an exponential distribution with the mean value of $\langle p_{Ti} \rangle$. The total contribution of two partons is the folding result of two exponential distributions. This results in the simplest Erlang distribution with the mean value of $2\langle p_{Ti} \rangle$ which can be extracted from the experimental transverse momentum distribution. Assuming an isotropic emission in the source rest frame, the rapidity and pseudorapidity distributions are obtained in the multisource picture. The parameter $\langle p_{Ti} \rangle$ reflects the violent degree of parton-parton collisions. Because of larger energy loss in the central region, the parton-parton collisions in the central region are more violent than those in the backward/forward regions.

From Figs. 2 and 3 we notice that, although the simplest Erlang distribution describes the mean trend of experimental p_T distribution in most cases, the theoretical curve seems to underestimate the tail part of the data, in particular for the last data. In fact, the simplest Erlang distribution does not describe the last two data simultaneously. To change this situation, we revise Eq. (2) to the simplest two-component Erlang distribution

$$f(p_T) = \frac{k_{1\text{st}} p_T}{\langle p_{Ti} \rangle_{1\text{st}}^2} \exp\left(-\frac{p_T}{\langle p_{Ti} \rangle_{1\text{st}}}\right) + \frac{(1 - k_{1\text{st}}) p_T}{\langle p_{Ti} \rangle_{2\text{nd}}^2} \exp\left(-\frac{p_T}{\langle p_{Ti} \rangle_{2\text{nd}}}\right), \quad (11)$$

where $k_{1\text{st}}$ denotes the contribution ratio (relative contribution) of the first component to the total one. Because J/ψ is believed to be produced via the hard process. Both the first and second components should correspond to hard processes. To give a distinction for the

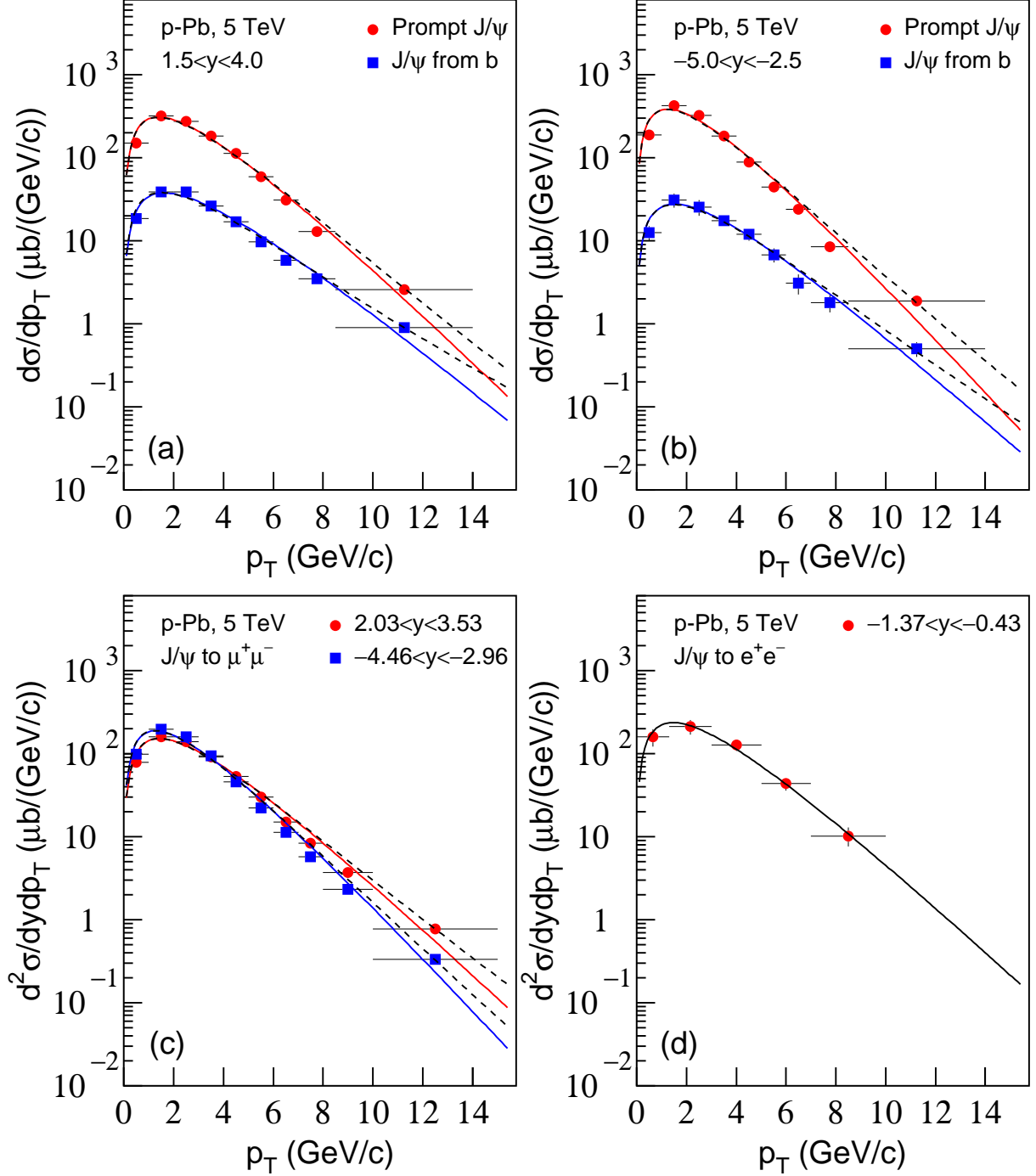


Fig. 2. (a)(b) Transverse momentum distributions of prompt J/ψ and J/ψ from b in rapidity ranges (a) $1.5 < y < 4.0$ and (b) $-5.0 < y < -2.5$ in p -Pb collisions at 5 TeV. The symbols represent the experimental data of the LHCb Collaboration [16] and the curves are our calculated results. (c)(d) Transverse momentum distributions of inclusive J/ψ to (c) $\mu^+\mu^-$ and (d) e^+e^- in p -Pb collisions at 5 TeV. The symbols represent the experimental data of the ALICE Collaboration [30] and the curves are our calculated results.

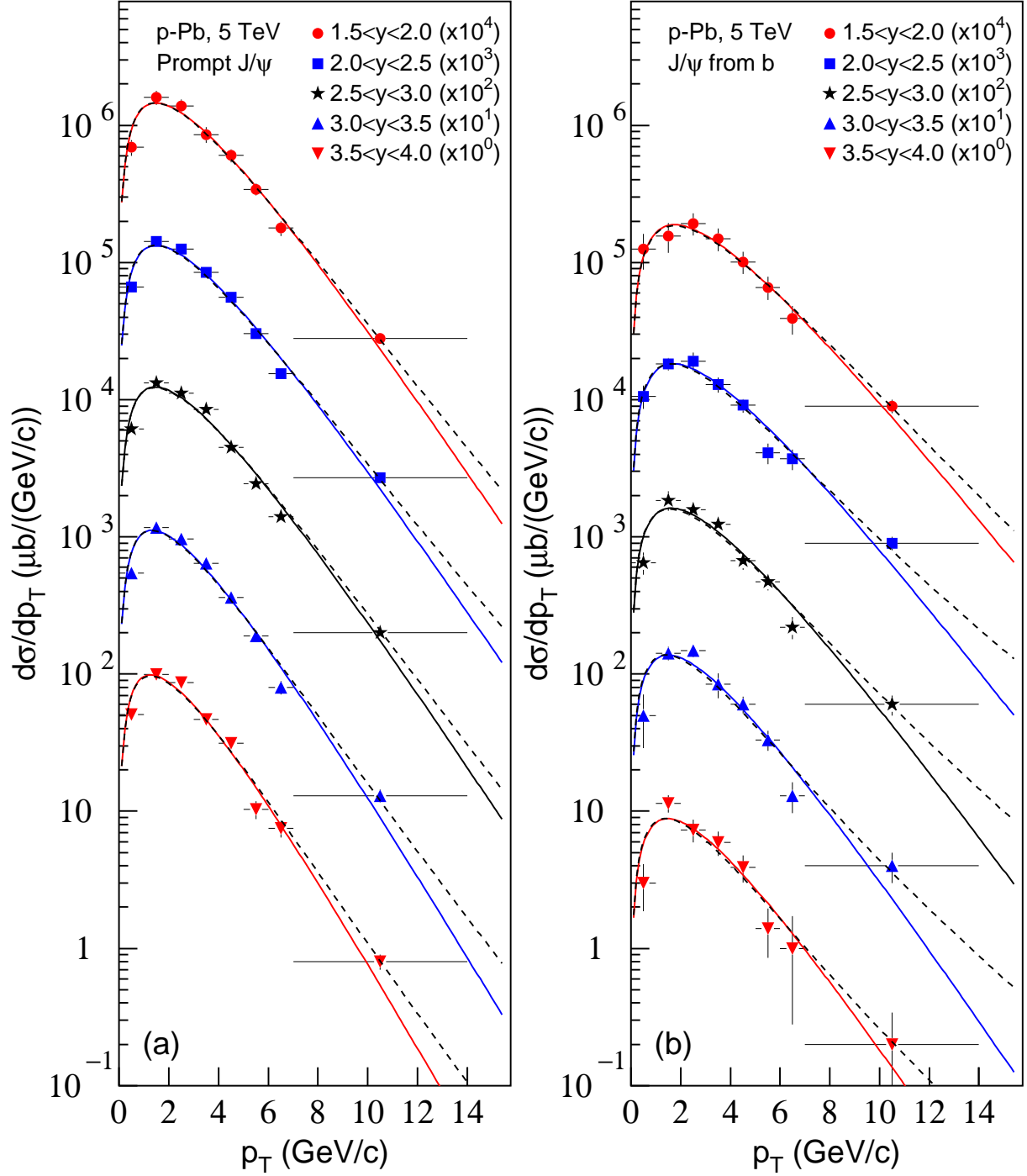


Fig. 3. Transverse momentum distributions of (a) prompt J/ψ and (b) J/ψ from b in different rapidity ranges in p -Pb collisions at 5 TeV. The symbols represent the experimental data of the LHCb Collaboration [16] and the curves are our calculated results.

two components, the first component is regarded as the hard “peripheral” parton-parton collisions, and the second one is regarded as the harder “central” parton-parton collisions. The mean transverse momentum $\langle p_T \rangle$ can be given by $2[k_{1st}\langle p_{Ti} \rangle_{1st} + (1 - k_{1st})\langle p_{Ti} \rangle_{2nd}]$.

By using the simplest two-component Erlang distribution, we recalculate and show the new p_T distributions by the dashed curves in Figs. 2 and 3. In the recalculation, we take $k_{1st} = 0.80 \pm 0.10$ and σ_0 to be the same as that in Table 1. Other parameters and χ^2/dof are listed in Table 2. One can see that both $\langle p_{Ti} \rangle_{1st}$ and $\langle p_{Ti} \rangle_{2nd}$ decrease with increase of the rapidity. The first component determines the peak position and the second one determines the tail slope. The violent degree of “peripheral” parton-parton collisions is lower than that of “central” parton-parton collisions.

In our recent work [33], we have used the similar picture and the same Erlang distribution to describe the transverse momentum distributions of light particles (π^\mp , K^\mp , \bar{p} , and p) produced in p -Pb collisions at 5 TeV and in Pb-Pb collisions at 2.76 TeV. The first component corresponds to the soft excitation process which has 2–5 partons to take part in the strong interactions. The second component corresponds to the hard scattering process which has 2 partons to take part in the violent collision. In the present work, for heavy particles such as J/ψ mesons and in terms of the two-component, both the numbers of partons corresponding to the first and second components are 2, and the first and second components correspond to hard and harder processes respectively. Although we have used different explanations for the first and second components in our previous and present works, they have the same formulism in principle.

The main goal of the present work is to study some universal laws existed in high energy collisions. The two-component Erlang distribution is one of the universal laws. It is known that hard QCD (Quantum Chromodynamics) contributions follow power law and not exponential (Erlang) distribution. The fits are very good the reason may be the two exponential (Erlang) slopes mimic a power law type behavior. In fact if one has a higher p_T data they may find a need of third (or more) exponential (Erlang) distribution with a third slope. Although we interpret the first term in Eq. (11) as soft and the second term as hard contribution in our earlier publication [33] which fits light hadrons, the present work treats heavy particles J/ψ and thus the first term is interpreted as hard and the second term as harder contribution. In fact, as one of the universal laws, the two-component Erlang distribution has more than one interpretations.

Although the production of some J/ψ 's can be explained as thermal recombination of primordially produced c and \bar{c} quarks at the hadronization transition [53], the present work does not limit the production process to thermal correlations such as equilibrium, local equilibrium, non-equilibrium, temperature, and so forth. Instead, we regard the exponential and Erlang distributions as statistical laws existed universally in particle collision and production, nuclear decay and fragmentation, mean free path, and other topics such as plant seed mass and size [54]. In these topics, many factors affect the results. Each factor contributes an exponential distribution. The contribution of many factors is the Erlang distribution which is the folding result of many exponential distributions. In addition, although the model used in the present work is called the multisource thermal model, it may not relate to thermal correlations. In fact, it can also be a statistical model. Not only for nucleus-nucleus and proton-nucleus collisions, but also for proton-proton and electron-positron collisions, the model can be applied in the case of statistical amount be-

ing high.

Table 2. Values of parameters and χ^2/dof corresponding to the dashed curves in Figs. 2 and 3. For all of the cases, $k_{1\text{st}} = 0.80 \pm 0.10$, σ_0 is the same as that in Table 1.

Fig.	Type or y range	$\langle p_{Ti} \rangle_{1\text{st}}$ (GeV/ c)	$\langle p_{Ti} \rangle_{2\text{nd}}$ (GeV/ c)	χ^2/dof
2(a)	prompt J/ψ	1.31 ± 0.07	1.80 ± 0.16	0.917
	J/ψ from b	1.45 ± 0.09	2.41 ± 0.29	0.291
2(b)	prompt J/ψ	1.16 ± 0.04	1.67 ± 0.14	1.161
	J/ψ from b	1.42 ± 0.09	2.10 ± 0.22	0.323
2(c)	$2.03 < y < 3.53$	1.33 ± 0.07	1.85 ± 0.17	0.913
	$-4.46 < y < -2.96$	1.18 ± 0.05	1.55 ± 0.10	0.877
3(a)	$1.5 < y < 2.0$	1.39 ± 0.08	1.92 ± 0.19	0.258
	$2.0 < y < 2.5$	1.39 ± 0.08	1.96 ± 0.20	0.415
	$2.5 < y < 3.0$	1.39 ± 0.08	1.82 ± 0.17	0.561
	$3.0 < y < 3.5$	1.25 ± 0.05	1.76 ± 0.16	0.682
	$3.5 < y < 4.0$	1.20 ± 0.04	1.69 ± 0.14	0.602
3(b)	$1.5 < y < 2.0$	1.65 ± 0.13	2.38 ± 0.28	0.125
	$2.0 < y < 2.5$	1.53 ± 0.11	2.65 ± 0.33	0.281
	$2.5 < y < 3.0$	1.48 ± 0.10	2.50 ± 0.30	0.487
	$3.0 < y < 3.5$	1.34 ± 0.07	2.39 ± 0.28	0.587
	$3.5 < y < 4.0$	1.33 ± 0.07	2.30 ± 0.26	0.532

It is noticed that the two- or multi-component Erlang distribution has wide applications. In our previous work [55], this distribution was used to describe multiplicity, mass, transverse mass, transverse energy, and transverse momentum spectra of final-state particles in proton-antiproton and electron-proton (positron-proton) collisions, as well as excitation energy spectrum for selected events in nucleus-nucleus collisions at high energies. This distribution was also used to describe the event-by-event fluctuations in the multiplicity, the total transverse energy, the mean transverse energy, and the mean transverse momentum in nucleus-nucleus collisions at high energies [22], and to describe the production cross-section of projectile-like isotopes in nucleus-nucleus collisions at intermediate and high energies [23, 24]. The present work uses this distribution to a wider range which deals with the hard process in J/ψ productions at the LHC.

4 Conclusions

We summarize here our main observations and conclusions.

(a) The rapidity distributions of prompt J/ψ , J/ψ from b , and inclusive J/ψ produced in asymmetric p -Pb collisions at 5 TeV can be described by the multisource thermal model. The sources for the three creations have nearly the same rapidity shifts in the uncertainty ranges in the backward target (Pb) and forward projectile (p) regions respectively, which renders that the three sources have the same contributors which are partons with the same collision energies. The rapidity shift in the backward Pb-region seems to be greater

than that in the forward p -region due to the target having a stronger penetrating power than the projectile.

(b) The pseudorapidity distributions of prompt J/ψ , J/ψ from b , and inclusive J/ψ produced in p -Pb collisions at 5 TeV are obtained from the parameter values extracted from the rapidity distributions. The obvious difference between the pseudorapidity and rapidity distributions is observed due to heavy particles. In fact, for heavy particles such as J/ψ mesons, we cannot neglect the difference between the two distributions even at the LHC energy. It is conceivable that the difference between the two distributions cannot be neglect at the lower GeV energy. The best treatment method in the calculation is to distinguish absolutely the rapidity and pseudorapidity distributions.

(c) In the considered range, the transverse momentum distributions of J/ψ mesons can be described by the simplest Erlang distribution which is the folding result of two exponential distributions which are contributed by target and projectile partons respectively. The extracted value of parameter $\langle p_{Ti} \rangle$ for J/ψ from b is greater than that for prompt J/ψ , and both the values decrease with increase of the rapidity. The Erlang distribution is an universal law existed in particle and nuclear physics, even in other fields of nature such as plant seed. To underline its physics behind is still an open question.

(d) The parameter $\langle p_{Ti} \rangle$ reflects the violent degree of parton-parton collisions. Because of larger energy loss in the central region, the parton-parton collisions in the central region are more violent than those in the backward/forward regions. The mean transverse momentum $\langle p_T \rangle$ can be given by $2\langle p_{Ti} \rangle$ due to the contributions of two partons. In terms of the two-component, both the numbers of partons corresponding to the first and second components are 2, and the first and second components correspond to hard and harder processes respectively. The mean transverse momentum $\langle p_T \rangle$ can be given by $2[k_{1st}\langle p_{Ti} \rangle_{1st} + (1 - k_{1st})\langle p_{Ti} \rangle_{2nd}]$.

Acknowledgment

This work was supported by the National Natural Science Foundation of China under Grant No. 11575103 and the US DOE under contract DE-FG02-87ER40331.A008.

References

- [1] Z.J. Jiang, J. Wang, K. Ma, H.L. Zhang, Adv. High Energy Phys. **2015**, 430606 (2015).
- [2] M. Nasim, V. Bairathi, M.K. Sharma, B. Mohanty, A. Bhasin, Adv. High Energy Phys. **2015**, 197930 (2015).
- [3] Z. Wazir, M.K. Suleymanov, B.Z. Belashev, S. Vokal, J. Vrláková, A. Zahir, S. Mehmood, M. Ajaz, S. Khalilova, M. Tufail, Indian J. Phys. **88**, 723 (2014).
- [4] P. Sett, P. Shukla, Adv. High Energy Phys. **2015**, 896037 (2015).
- [5] R.C. Hwa, Adv. High Energy Phys. **2015**, 526908 (2015).

- [6] S. Chatterjee, S. Das, L. Kumar, D. Mishra, B. Mohanty, R. Sahoo, N. Sharma, Adv. High Energy Phys. **2015**, 349013 (2015).
- [7] G.-Y. Qin, Int. J. Mod. Phys. E **24**, 1530001 (2015).
- [8] H.-T. Ding, F. Karsch, S. Mukherjee, Int. J. Mod. Phys. E **24**, 1530007 (2015).
- [9] H. Song, S.A. Bass, U. Heinz, T. Hirano, C. Shen, Phys. Rev. Lett. **106**, 192301 (2011).
- [10] J. Novak, K. Novak, S. Pratt, J. Vredevoogd, C. Coleman-Smith, R. Wolpert, Phys. Rev. C **89**, 034917 (2014).
- [11] A. Andronic, Int. J. Mod. Phys. A **29**, 1430047 (2014).
- [12] PHENIX Collaboration (A. Adare *et al.*), Phys. Rev. Lett. **107**, 142301 (2011).
- [13] PHENIX Collaboration (S.S. Adler *et al.*), Phys. Rev. Lett. **94**, 082302 (2005).
- [14] BRAHMS Collaboration (I. Arsene *et al.*), Phys. Rev. Lett. **93**, 242303 (2004).
- [15] ALICE Collaboration (B. Abelev *et al.*), Phys. Lett. B **718**, 1273 (2013).
- [16] LHCb Collaboration (R. Aaij *et al.*), JHEP **02**, 072 (2014).
- [17] A. Rakotozafindrabe, E.G. Ferreira, F. Fleuret, J.P. Lansberg, J. Phys. G **37**, 094055 (2010).
- [18] E.G. Ferreira, F. Fleuret, J.P. Lansberg, N. Matagne, A. Rakotozafindrabe, Nucl. Phys. A **855**, 327 (2011).
- [19] R. Vogt, Phys. Rev. C **81**, 044903 (2010).
- [20] E.G. Ferreira, Phys. Lett. B **731**, 57 (2014).
- [21] S. Ganesh, M. Mishra, Nucl. Phys. A **947**, 38 (2016).
- [22] Q.-W. Lü, L.-L. Liu, F.-H. Liu, N. N. Abd Allah, J. Korean Phys. Soc. **59**, 2684 (2011).
- [23] Y.-Q. Gao, Z.-X. Zhang, Y.-Y. Zhao, F.-H. Liu, J. Korean Phys. Soc. **60**, 1011 (2012).
- [24] F.-H. Liu, J.-S. Li, Phys. Rev. C **78**, 044602 (2008).
- [25] S. Kaur, R.K. Puri, Phys. Rev. C **89**, 057603 (2014).
- [26] S. Kaur, R.K. Puri, Phys. Rev. C **90**, 037602 (2014).
- [27] LHCb Collaboration (R. Aaij *et al.*), Eur. Phys. J. C **71**, 1645 (2011).
- [28] LHCb Collaboration (R. Aaij *et al.*), JHEP **02**, 41 (2013).

- [29] ALICE Collaboration (B. Abelev *et al.*), JHEP **06**, 073 (2014).
- [30] ALICE Collaboration (J. Adam *et al.*), JHEP **06**, 55 (2015).
- [31] F.-H. Liu, Phys. Lett. B **583**, 68 (2004).
- [32] F.-H. Liu, Phys. Rev. C **78**, 014902 (2008).
- [33] F.-H. Liu, Y.-Q. Gao, T. Tian, B.-C. Li, Eur. Phys. J. A **50**, 94 (2014).
- [34] F.-H. Liu, Y.A. Panebratsev, Phys. Rev. C **59**, 1798 (1999).
- [35] F.-H. Liu, Y.A. Panebratsev, Phys. Rev. C **59**, 1193 (1999).
- [36] K. Werner, Phys. Rep. **232**, 87 (1995).
- [37] G.D. Westfall *et al.*, Phys. Rev. Lett. **37**, 1202 (1976).
- [38] A. D’innocenzo, G. Ingrosso, P. Rotelli, Nuovo Cimento A **44**, 375 (1978).
- [39] A. D’innocenzo, G. Ingrosso, P. Rotelli, Lett. Nuovo Cimento **25**, 393 (1979).
- [40] A. D’innocenzo, G. Ingrosso, P. Rotelli, Nuovo Cimento A **55**, 417 (1980).
- [41] A. D’innocenzo, G. Ingrosso, P. Rotelli, Lett. Nuovo Cimento **27**, 457 (1980).
- [42] L.-S. Liu, T.-C. Meng, Phys. Rev. D **27**, 2640 (1983).
- [43] K.-C. Chou, L.-S. Liu and T.-C. Meng, Phys. Rev. D **28**, 1080 (1983).
- [44] G. Wolschin, Eur. Phys. J. A **5**, 85 (1999).
- [45] G. Wolschin, Prog. Part. Nucl. Phys. **59**, 374 (2007).
- [46] G. Wolschin, EPL **95**, 61001 (2011).
- [47] G. Wolschin, J. Phys. G **40**, 045104 (2013).
- [48] F.-H. Liu, Chin. J. Phys. **42**, 694 (2004).
- [49] L.-N. Gao, F.-H. Liu, Adv. High Energy Phys. **2015**, 184713 (2015).
- [50] L.-K. Ding, B. Andersson, G. Gustafson, E. Stenlund, High Energy Phys. Nucl. Phys. (Chin. Phys. C) **14**, 303 (1990).
- [51] S. Date, M. Gyulassy, H. Sumiyoshi, Phys. Rev. D **32**, 619 (1985).
- [52] F.-H. Liu, Y.-H. Chen, Y.-Q. Gao, E.-Q. Wang, Adv. High Energy Phys. **2013**, 710534 (2013).
- [53] L. Grandchamp, R. Rapp, Phys. Lett. B **523**, 60 (2001).
- [54] S.-H. Fan, H.-R. Wei, J. Kor. Phys. Soc. **61**, 1918 (2012).
- [55] E.-Q. Wang, H.-R. Wei, M. A. Rahim, S. Fakhreddin, F.-H. Liu, Indian J. Phys. **87**, 185 (2013).